Bioelectrochemistry 89 (2013) 50–56

Contents lists available at SciVerse ScienceDirect

Bioelectrochemistry

journal homepage: www.elsevier.com/locate/bioelechem

Triazole–acridine conjugates: Redox mechanisms and *in situ* electrochemical evaluation of interaction with double-stranded DNA

A. Dora R. Pontinha [a], Silvia Sparapani [b], Stephen Neidle [b], Ana Maria Oliveira-Brett [a,*]

[a] Departamento de Química, Faculdade de Ciências e Tecnologia, Universidade de Coimbra, 3004-535 Coimbra, Portugal
[b] CRUK Biomolecular Structure Group, UCL School of Pharmacy, University College London, London WC1N 1AX, UK

ARTICLE INFO

Article history:
Received 3 May 2012
Received in revised form 8 August 2012
Accepted 9 August 2012
Available online 11 September 2012

Keywords:
Disubstituted triazole-linked acridines
GL15
GL7
Electrochemistry
DNA

ABSTRACT

Redox mechanisms and in situ electrochemical interaction with double-stranded DNA were investigated using a DNA-electrochemical biosensor for two disubstituted triazole-linked acridine compounds (GL15 and GL7), previously reporting as quadruplex DNA-binding molecules. The redox properties of GL15 and GL7 involve a complex, pH-dependent, adsorption-controlled irreversible process and were investigated using cyclic, differential pulse, and square wave voltammetry at a glassy carbon electrode. The interaction between duplex DNA and GL15 or GL7 was investigated in incubated solutions using dsDNA-, poly[G]-, and poly[A]-electrochemical biosensors. It was demonstrated that the interaction is time-dependent, both GL15 and GL7 interacting with dsDNA, causing condensation of dsDNA morphological structure but not oxidative damage.

1. Introduction

Telomeres and their associated proteins are specialized structures at the ends of linear chromosomes that function by protecting double-stranded DNA (dsDNA) from recombination, degradation and end-to-end fusions [1,2]. The formation of G-quadruplex-DNA at the end of telomeric DNA increases genomic instability [2,3], and also inhibits telomerase activity [4]. This in turn induces cellular senescence and cell death in cancer cells [5,6]. The use of small molecules able to induce and stabilize G-quadruplex arrangements can promote telomerase inhibition and telomere dysfunction in cancer cells [7–11], thus providing a broad therapeutic selectivity. The binding affinity and selectivity of these molecules depend on properties of both the chromophores and substituted groups [12].

Acridines are heterocyclic structures widely studied as antitumor, antiparasitic and antibacterial agents [13], a number of which have been shown to stabilize quadruplex DNA structures. A great diversity of acridine derivatives has been synthesized with the purpose of significantly increasing binding affinity and selectivity for human telomeric quadruplex [11,14,15]. The core polyaromatic ring of acridines has a high affinity for dsDNA leading to intercalation and stacking [8] and a recently-designed series of disubstituted triazole-linked acridine compounds has shown selectivity to human telomeric sequences [11].

Several quadruplex-targeting acridine derivatives, BRACO-19 and RHPS4, have been important tools for studying the antitumor activity of this general class of agents, but neither is totally quadruplex-selective [16]. The acridine chromophore is bound in a stacking arrangement with quadruplex DNAs that is distinct from intercalation into dsDNA, even though its extended electron-deficient aromatic ring system enables it to form strong π–π stacking interactions with nucleobases. Generally chromophores prefer to bind on the exterior of the guanine-tetrad stacks in a quadruplex, whether or not the strands are all-parallel [17–19].

Electrochemical techniques, such as pulse techniques, are suitable for studies of biological systems, with very little or no sample pre-treatment, and have been successfully used for the detection and determination of several pharmaceutical drugs since they are fast and have high sensitivity [20–23].

A dsDNA-electrochemical biosensor is an integrated receptor-transducer device that uses dsDNA as a biomolecular recognition element to measure specific binding processes with dsDNA, through electrochemical transduction. The most important factor for the construction of efficient dsDNA-electrochemical biosensors is the immobilization of the dsDNA probe on the electrode surface. Different adsorption immobilization procedures, electrostatic adsorption or evaporation, forming monolayer or multilayer DNA films have been used. The multilayer dsDNA-electrochemical biosensor consists of

* Corresponding author at: Departamento de Quíımica, Faculdade de Ciências e Tecnologia, Universidade de Coimbra, 3004-535 Coimbra, Portugal. Tel./fax: +351 239 835295.
E-mail address: brett@ci.uc.pt (A.M. Oliveira-Brett).

1567-5394/$ – see front matter © 2012 Elsevier B.V. All rights reserved.
http://dx.doi.org/10.1016/j.bioelechem.2012.08.005

an electrode with dsDNA deposited on the transducer surface by successive monolayer coverage [24].

The dsDNA-electrochemical biosensor, using differential pulse voltammetry, has been successfully utilized to investigate the interaction of small molecules, heavy metals and other hazardous compounds with dsDNA [25], and compared with other methods shows greater sensitivity in the detection of small perturbations of the double-helical morphological structure of DNA and the detection of DNA oxidative damage, enabling the unravelling of detailed mechanistic interactions.

Another important advantage of using dsDNA-electrochemical biosensors is the possibility of generation of highly reactive intermediates in situ, on the electrode surface, and the electrochemical detection of their direct interaction with dsDNA. It has been successfully applied to study the interaction of a number of substances with dsDNA and the interpretation of the results contributed to the elucidation of the mechanisms by which DNA is damaged by hazardous compounds [26].

Two members of a series of triazole–acridine conjugate compounds, designated as GL15 and GL7, Scheme 1, that bind with high selectivity to telomeric quadruplex DNA, were chosen for this study [11], which has investigated their *in situ* interaction with dsDNA, The aim is to provide new data concerning DNA damage, as well as on GL15 and GL7 oxidation and reduction mechanisms.

To clarify the nature of the interaction between GL15 and GL7 and dsDNA, similar experiments were also performed using polyribonucleotides of known sequences, and poly[G]- and poly [A]-electrochemical biosensors were prepared. This approach has been used for the understanding of preferential dsDNA base interactions with complex agents and individual chemicals of environmental, food and medical relevance [27]. Although, poly[G] and poly[A] are different from dsDNA the preferential interaction of a compound with a specific base is similar.

2. Experimental

2.1. Materials and reagents

The triazole–acridine conjugates, GL15 and GL7, were synthesized and purified as previously published [11]. Double stranded DNA (dsDNA), polyadenylic acid (poly[A]) and polyguanylic acid (poly[G]) were from Sigma-Aldrich, and were all used without further purification.

The 0.1 M ionic strength electrolyte solutions were: pH 2.0 KCl/HCl, pH 3.4–5.4 acetate buffer, pH 6.1–8.0 phosphate buffer, pH 9.2–10.5 amonia buffer, and pH 12.0 NaOH/KCl were prepared using analytical grade reagents and purified water from a Millipore Milli-Q system (conductivity ≤ 10 μS m^{-1}).

Stock solutions of 0.3078 mM GL15 and GL7 were prepared in deionized water, adding some drops of 0.2 M HCl, and stored at 5 °C. Solutions of different concentrations were obtained by dilution of the appropriate volume in the supporting electrolyte.

Stock solutions of 151 μg mL^{-1} dsDNA, 477 μg mL^{-1} poly[G], and 587 μg mL^{-1} poly[A] were prepared in deionized water and diluted to the desired concentrations in pH = 7.0 (0.1 M phosphate buffer).

Nitrogen saturated solutions were obtained by bubbling high purity N_2 for a minimum of 10 min in the solution and continuing with a flow of pure gas over the solution during the voltammetric experiments to avoid oxygen in the solution.

Microvolumes were measured using EP-10 and EP-100 Plus Motorized Microliter Pippettes (Rainin Instrument Co. Inc., Woburn, USA). The pH measurements were carried out with a Crison micropH 2001 pH-meter with an Ingold combined glass electrode.

All experiments were done at room temperature (25 ± 1 °C).

2.2. Voltammetric parameters and electrochemical cells

Voltammetric experiments were carried out using a μAutolab potentiostat with GPES 4.9 software (Eco-Chemie, Utrecht, The Netherlands). The measurements were carried out in a solution volume of 0.5 mL, using a three-electrode system one-compartment electrochemical cell of capacity 2 mL (Cypress System Inc., USA). A glass carbon electrode (GCE, $d = 1.5$ mm) was the working electrode, a Pt wire the counter electrode and an Ag/AgCl (3 M KCl) reference electrode. The experimental conditions were: for cyclic voltammetry (CV) scan rate 100 mV s^{-1}, and for differential pulse (DP) voltammetry pulse amplitude 50 mV, pulse width 70 ms and scan rate 5 mV s^{-1}.

The GCE was polished using a diamond spray (particle size 3 μm) (Kemet, UK) before each electrochemical experiment. After polishing, it was rinsed thoroughly with Milli-Q water. Following this mechanical treatment, the GCE was placed in buffer supporting electrolyte and differential pulse voltammograms were recorded until a steady state baseline voltammogram was obtained. This procedure ensured very reproducible experimental results.

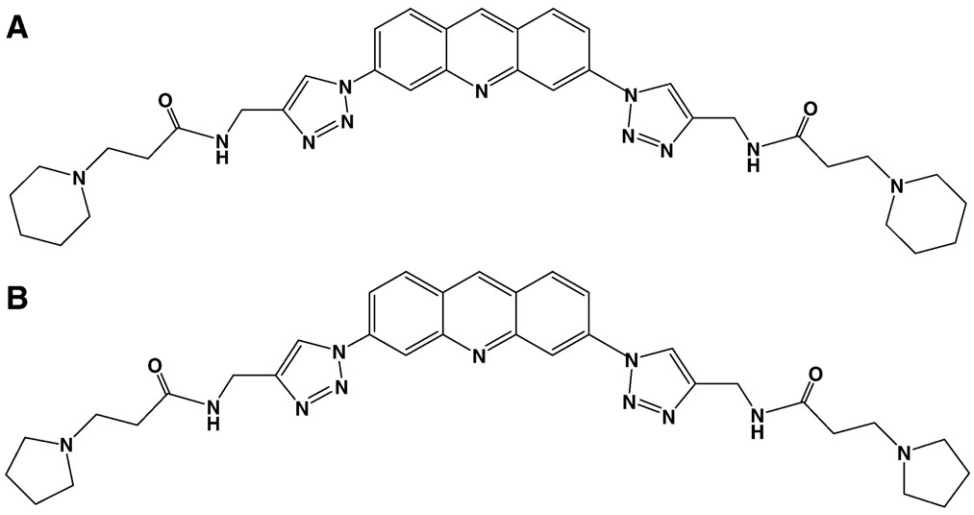

Scheme 1. Chemical structures: (A) GL15 and (B) GL7.

2.3. Acquisition and presentation of voltammetric data

Differential pulse voltammograms presented were background-subtracted and baseline-corrected using the moving average application with a step window of 5 mV included in the GPES version 4.9 software. This mathematical treatment improves the visualization and identification of peaks over the baseline without introducing any artefact, although the peak intensity is, in some cases, reduced (<10%) relative to that of the untreated curve. Nevertheless, this mathematical treatment of the original voltammograms was used in the presentation of all experimental voltammograms for an improved and clearer identification of the peaks. The values for peak current presented in all plots were determined from the original untreated voltammograms after subtraction of the baseline.

2.4. DNA-biosensor preparation and incubation procedure

The multi-layer dsDNA-electrochemical biosensor, poly[A]- and poly[G]-electrochemical biosensors were prepared by electrostatic immobilization, covering the GCE ($d = 1.5$ mm) surface with three drops of 5 μL each of 50 μg mL^{-1} dsDNA, poly[A] or poly[G] solutions. After placing each drop on the electrode surface the electrochemical biosensor was dried under a constant flux of N_2, and afterwards a potential of +0.30 V vs. Ag/AgCl was applied during 5 min.

The multilayers of DNA, polyA and polyG, are very easily immobilized by adsorption on the glassy carbon electrode surface. As all the experiments are with a positive applied potential there is no partial desorption of DNA, polyA and polyG.

Incubations were always carried out, during different periods of time, by immersing the electrochemical biosensors in pH = 7.0 (0.1 M phosphate buffer) solutions containing 50 μM GL15 or GL7 under continuously stirring.

3. Results and discussion

The redox behavior of the triazole–acridine conjugates GL15 and GL7 was studied first, followed by investigation of the in situ interaction of them with dsDNA, using dsDNA-electrochemical biosensors and incubated solutions.

3.1. Redox behavior of GL15 and GL7

The electrochemical behavior of GL15 and GL7 was investigated using CV in pH = 7.0 (0.1 M phosphate buffer) in N_2 saturated solutions using a GCE. CVs were recorded in the interval, −1.1 V to +1.0 V, always starting at 0.0 V (Fig. 1). The results showed that both GL15 and GL7 undergo oxidation and reduction. However, since the redox processes occur independently of each other they were investigated separately.

3.1.1. Oxidation

3.1.1.1. Cyclic voltammetry. The oxidation behavior of 50 μM GL15 was studied in pH = 7.0 (0.1 M phosphate buffer) by CV at a scan rate $\nu = 100$ mV s^{-1}. The first CV showed one anodic peak on the first positive-going scan, peak 1_a, at $E_{p1a} = +0.89$ V (Fig. 1A). Reversing scanning in the negative direction, no reduction peak was observed, indicating that the oxidation process of GL15 is irreversible. Successive CVs showed a large decrease of the oxidation currents of peak 1a due to the adsorption of GL15 and/or its non-electroactive oxidation products on the GCE surface.

The oxidation behavior of 50 μM GL7 was investigated under the same conditions. The first CV showed two irreversible peaks on the first positive-going scan, peak 1_a, at $E_{p1a} = +0.76$ V, and peak 2_a, at $E_{p2a} = +0.88$ V (Fig. 1B). CVs were also obtained for different scan rates. By increasing the scan rate, for both compounds, peak 1_a current increased, following a linear relationship with scan rate as expected for an adsorbed species reaction. Between each measurement, the electrode surface was always polished in order to ensure a clean surface and to avoid possible problems due to adsorption.

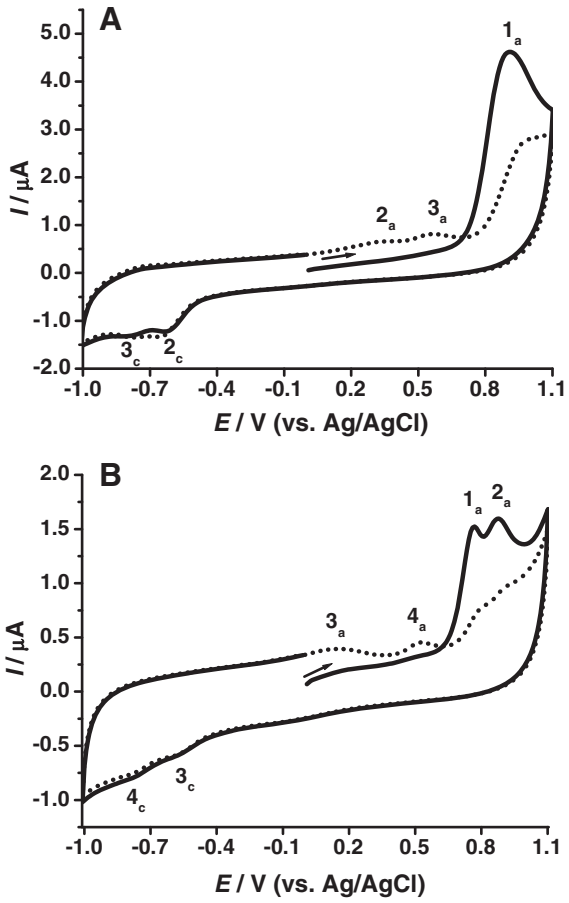

Fig. 1. CVs with a GCE in a N_2 saturated solution in pH = 7.0 0.1 M phosphate buffer: (A) 50 μM GL15 and (B) 50 μM GL7, (—) first and (•••) second scans, at $\nu = 100$ mV s^{-1}.

3.1.1.2. Differential pulse voltammetry and effect of pH. DP voltammograms for the oxidation of 4 μM GL15 and 10 μM GL7 were obtained in aqueous buffer supporting electrolytes 2.0 < pH < 12.0 (Fig. 2).

The peak 1a for GL15 occurs in all supporting electrolytes (Fig. 2A). The potential of peak 1a is shifted to more negative values with increasing pH. The slope of the E_{p1a} vs. pH, dotted line 59 mV per pH unit (Fig. 2B) shows that the mechanism of this oxidation process in aqueous media involves the same number of electrons and protons. The half-height width of peak 1_a, $W_{1/2} = 90$ mV, is close to the theoretical value for the transfer of one electron [28], so the oxidation of GL15 occurs with the transfer of one electron and one proton.

The peaks 1_a and 2_a for GL7 occur for all experimental conditions and their potential decreases with increasing pH (Fig. 2C). The slope of the E_{p1a} vs. pH, dotted line 59 mV per pH unit (Fig. 2D) shows that the same number of electrons and protons are involved in the oxidation mechanism (Fig. 2D) but as $W_{1/2} = 60$ mV, the peak 1_a GL7 oxidation occurs with the transfer of two electrons and two protons.

3.1.2. Reduction

3.1.2.1. Cyclic voltammetry. The reduction of 30 μM GL15 and 30 μM GL7 was investigated by CV, starting at 0.0 V to −1.0 V and reversing

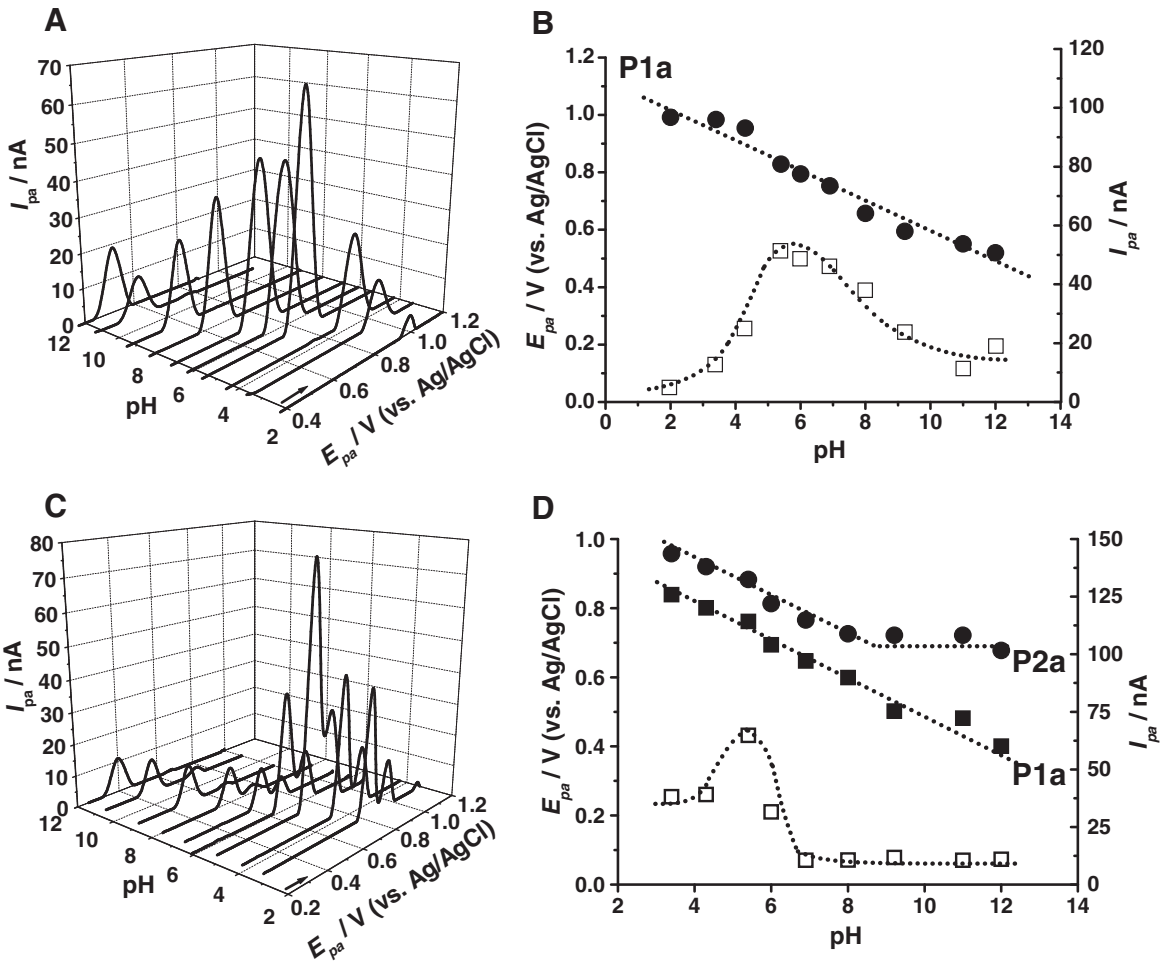

Fig. 2. Plots as a function of pH of the supporting electrolyte: (A) first scan 3D base-line corrected DP voltammograms of 4 μM GL15; (B) E_{pa} (●) and I_{pa} (□) of peak 1_a vs. pH of GL15; and (C) first scan 3D base-line corrected DP voltammograms of 10 μM GL7; (D) E_{pa} of: (■) peak 1_a and (●) peak 2_a and I_{pa} (□) of peak 1_a vs. pH of GL7.

until +0.7 V, in pH = 6.0 (0.1 M phosphate buffer), N_2 saturated, at scan rate $\nu = 100$ mV s^{-1}. The reduction of GL15 showed two peaks, peak 2_c at $E_{p2c} = -0.47$ V and peak 3_c at $E_{p3c} = -0.76$ V (Fig. 3); reversing the scan direction, the correspondent anodic peak 2_a at $E_{p2a} = +0.23$ V, and peak 3_a at $E_{p3a} = +0.52$ V, appeared. The difference $|E_{p2c} - E_{p2a}| = \sim 80$ mV and $|E_{p3c} - E_{p3a}| = \sim 128$ mV, indicates the quasi-reversibility of GL15 reduction.

The reduction of GL7 was very similar to that of GL15. On the negative-going scan two peaks were observed, peak 3_c, at $E_{p3c} = -0.53$ V, and peak 4_c, at $E_{p4c} = -0.77$ V, and reversing the scan direction, the corresponding anodic peak 3_a, at $E_{p3a} = +0.18$ V, and peak 4_a, at $E_{p4a} = +0.47$ V, appeared.

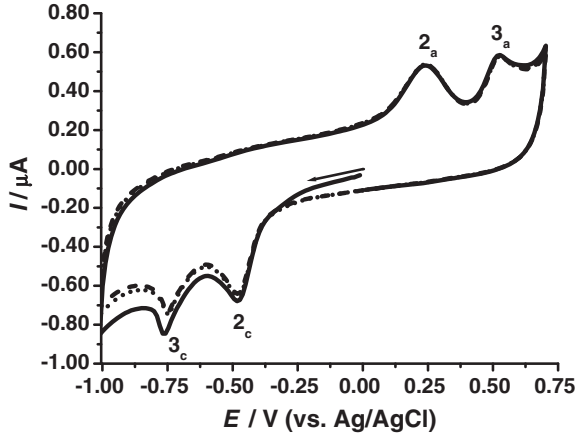

Fig. 3. CVs with a GCE in N_2 saturated solutions of 30 μM GL15 in pH = 6.1 0.1 M phosphate buffer; (—) first and (•••) second and (- - -) third scan, at $\nu = 100$ mV s^{-1}.

3.1.2.2. Differential pulse voltammetry and pH effect. The reduction of the two compounds GL15 and GL7, was investigated for 2.0 < pH < 12.0 in N_2 saturated buffer supporting electrolyte solutions by DP voltammetry (Fig. 4).

The DP voltammograms of 10 μM GL15 showed two reduction peaks, peak 2_c and peak 3_c in all supporting electrolytes. For pH < 9.0, both peak potentials were shifted to more negative values with increasing pH (Fig. 4A). The dependence followed the relationship E_{p2c} (V) = −0.042 - 0.060 pH for peak 2_c, and E_{p3c} (V) = −0.021 - 0.060 pH for peak 3_c (Fig. 4C) indicating that the reduction mechanism in both peaks occurs with the transfer of the same number of electrons and protons. As for peak 2_c, $W_{1/2} = 90$ mV, and for peak 3_c, $W_{1/2} = 103$ mV, the reduction of GL15 amino groups occur in two steps each with the transfer of one electron and one proton, Scheme 2.

For pH > 9.0, the reduction of GL15 is pH-independent with a mechanism involving only one electron. The GL15 reduction product can undergo chemical deprotonation in alkaline electrolytes [29] and the value of $pK_a = 9$ for GL15 was determined. DP voltammograms of

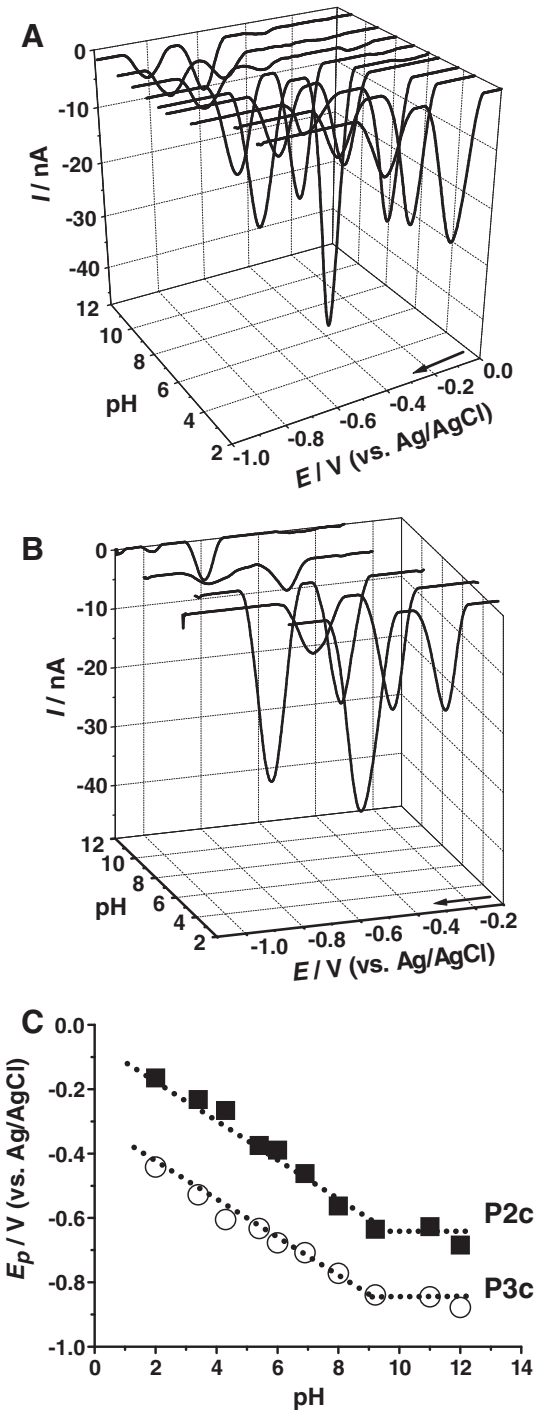

Fig. 4. Plots as a function of pH of the supporting electrolyte in N_2 saturated in 10 μM: (A) GL15 and (B) GL7, 3D base-line corrected DP voltammograms; (C) E_{pc} of (■) peak 2_c and (○) peak 3_c vs. pH of GL15.

10 μM GL7 showed two reduction peaks, peak 3_c and 4_c (Fig. 4B) following the relationships: E_{p3c} (V) = −0.072 - 0.060 pH for peak 3_c and $W_{1/2}$ = 82 mV, and E_{p4c} (V) = −0.32 - 0.060 pH for peak 4_c and $W_{1/2}$ = 116 mV, which correspond to reduction mechanisms with the transfer of one electron and one proton.

3.2. Triazole–acridine conjugates–dsDNA interaction

The interaction between dsDNA and the triazole–acridine conjugates, GL15 and GL7, was investigated using dsDNA-, poly[G]-, and poly[A]-electrochemical biosensors and in incubated solutions.

3.2.1. Study in triazole–acridine conjugates–dsDNA incubated solutions

The ease of protonation of acridine derivatives at physiological pH is known to have an influence on their antimicrobial activity [30] and interaction with DNA [31].

DP voltammograms recorded in incubated solutions, as described in Section 2.4, were registered after incubation periods of 0, 2, 3 and 5 h. The GCE surface was always cleaned between each measurement to avoid blocking of the surface by adsorption of electroactive species or their oxidation products.

The oxidation behavior of dsDNA in pH = 7.0 (0.1 M phosphate buffer) using DP voltammetry was the control in order to clarify the GL15 and GL7 interaction with dsDNA.

The DP voltammogram of dsDNA control showed two peaks, that do not change with time, corresponding to the oxidation of desoxyguanosine (dGuo), at E_{pa} = +0.92 V, and desoxyadenosine (dAdo), at E_{pa} = +1.17 V (Fig. 5). The DP voltammograms of dsDNA show smaller oxidation peak currents, due to the difficulty of the electron transfer from the inside of the double-stranded rigid form of DNA to the electrode surface.

The DP voltammograms of 4 μM GL15 with 100 μg mL^{-1} dsDNA recorded immediately after addition of GL15 to the dsDNA solution, showed three peaks due to the oxidation of purinic dsDNA bases dGuo, at E_{pa} = +0.91 V, dAdo, at E_{pa} = +1.17 V and GL15 oxidation, at E_{pa} = +0.77 V (Fig. 5). Increasing the incubation time, the peak currents corresponding to guanine and adenine oxidation decreased compared with those obtained for the control dsDNA solution. This indicates that dsDNA condensed after the GL15–DNA interaction, and consequently electron transfer to the electrode surface is more difficult, explaining the decrease in the guanine and adenine oxidation peaks.

AFM results and the voltammetric data have previously demonstrated that drugs, hazardous and biological compounds interact specifically with dsDNA [32,33], with some compounds forming covalent bonds with nitrogenous bases, and inducing structural changes in B-DNA. The reorganization of the DNA self-assembled network on the surface electrode has been investigated by AFM. Local denaturation of the double helix due to compound–DNA interaction facilitating the hydrophobic interactions between the DNA bases and the hydrophobic carbon electrode surface was observed. Conformational modifications of the dsDNA double helix and the formation of thicker aggregates caused by DNA condensation [32], inducing large morphological changes in the DNA adsorption pattern, were observed by AFM and also confirmed by the decrease in the guanine and adenine oxidation peaks in the voltammetric results.

No additional peaks, such as for the biomarkers 8-oxoguanine or 2,8-oxoadenine, the oxidation products of guanine or adenine, were observed in the DP voltammograms, so it was concluded that in the experimental conditions using GL15 interacts with dsDNA but does not cause oxidative damage to DNA.

3.2.2. Study of in situ triazole–acridine conjugates–DNA interaction using electrochemical biosensors

The interaction between the triazole–acridine conjugates GL15 and GL7 and various nucleic acids, was investigated using dsDNA-, poly[G]-, and poly[A]-electrochemical biosensors.

The dsDNA-electrochemical biosensor consists of an electrode with dsDNA immobilized on the surface. The interaction of the compound with surface-immobilized dsDNA resulted in changes in DNA morphology which can be followed by the changes in the oxidation peaks of dsDNA purine bases dGuo, at E_{pa} = +0.91 V, dAdo, at E_{pa} = +1.17 V. Changes caused *in situ* to the dsDNA immobilized on the electrode surface during interaction with GL15 were followed in real time by DP voltammetry using a multilayer dsDNA-electrochemical biosensor prepared as described in Section 2.4.

The dsDNA-electrochemical biosensor was incubated for 3 min with 50 μM GL15, washed carefully with deionized water to remove

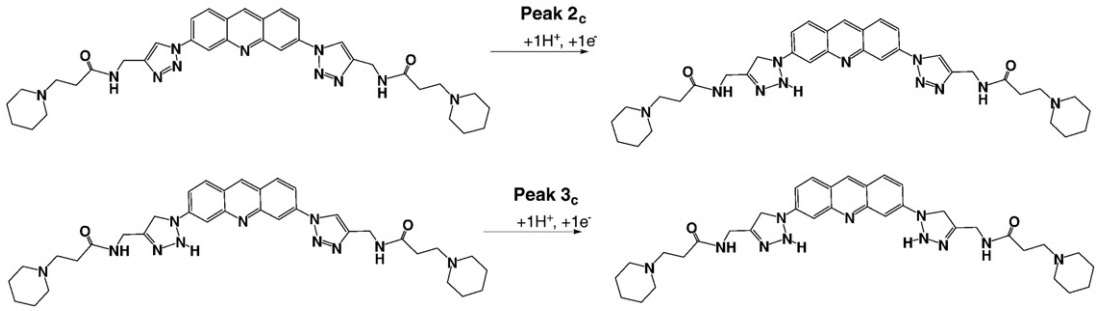

Scheme 2. Proposed mechanism for reduction of GL15.

unbounded GL15 molecules and transferred to phosphate buffer, where a DP voltammogram was recorded (Fig. 6). The DP voltammograms showed the GL15 peak followed by the dsDNA peaks due to oxidation of the purine bases guanine and adenine.

This experiment was repeated, always using a newly-prepared biosensor, for incubation times of 5, 7 and 10 min. A progressive decrease of dsDNA base oxidation peaks, with increasing incubation time, was observed. The decrease in guanine and adenine oxidation peaks corresponds to the condensation of dsDNA morphology.

No oxidative DNA damage occurred during the GL15–dsDNA interaction, since no peaks corresponding to 8-oxoguanine or 2,8-oxoadenine were observed. The GL15 oxidation peak increased with time due to incorporation and pre-concentration into the DNA film.

Similar experiments were performed using polyribonucleotides of known sequences with poly[G]- and poly[A]-electrochemical biosensors to obtain more information about the preferential interaction of purine bases, guanine or adenine, with dsDNA structure.

The control poly[A]-electrochemical biosensor showed the oxidation of adenine, with a peak at $E_{pa} = +1.15$ V (Fig. 7A). Freshly-prepared poly[A]-electrochemical biosensors were incubated with 50 μM GL15 during different periods of time. The peak corresponding to the oxidation of adenine remained constant and the GL15 oxidation peak decreased with increasing incubation time (Fig. 7A).

The control poly[G]-electrochemical biosensor showed the oxidation of guanine, with a peak at $E_{pa} = +0.91$ V (Fig. 7B). Freshly-prepared poly[G]-electrochemical biosensors were incubated with 50 μM GL15. The guanine peak decreased and the GL15 peak increased with increasing incubation time. This increase in the GL15 peak is explained by the occurrence of free guanine released from the DNA, at $E_{pa} = +0.70$ V, the same potential as GL15 oxidation, showing DNA damage but, as no 8-oxoguanine was detected, no DNA oxidative damage occurred.

Similar behavior was observed for GL7 interacting with the dsDNA-electrochemical biosensor.

The interaction of GL15 and GL7 with dsDNA is not selective for a specific DNA base, does not involve oxidative damage, but there is an indication of preferential interaction with guanine-rich DNA sequences, that was found using the poly[G]-electrochemical biosensor (Fig. 7B).

4. Conclusions

The electrochemical investigation of disubstituted triazole-linked acridine compounds, GL15 and GL7 has provided valuable insights into the biological redox reactions of these molecules. This was carried out over a wide pH range and showed that they undergo oxidation and reduction at a GCE. Their oxidation is an irreversible and pH-dependent process that for GL15 occurs in one step with the transfer of one electron and one proton, and for GL7 in two steps with the transfer of two electrons and two protons. The reduction of both compounds is similar in that both involve quasi-reversible pH-dependent process which involves the transfer of one electron and one proton.

The interaction between DNA and the acridine ligands was investigated in incubated solutions and using double-stranded DNA-, poly [G]-, and poly[A]-electrochemical biosensors. Both GL15 and GL7 interact with dsDNA with increasing incubation time, causing condensation of the dsDNA morphological structure, with preferential affinity for guanine rich segments but do not cause oxidative damage.

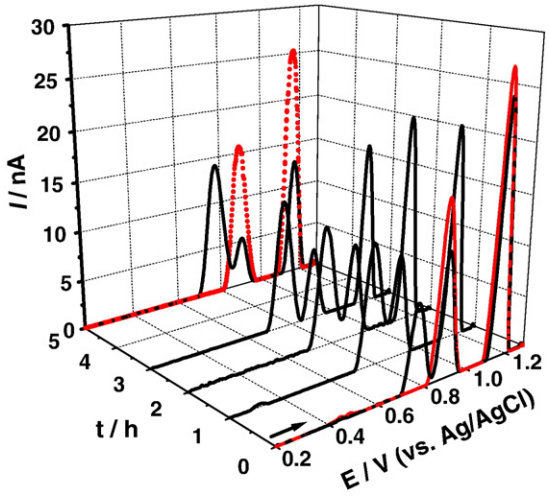

Fig. 5. DP voltammograms base-line corrected in pH = 7.0 0.1 M phosphate buffer solutions: 100 μg mL^{-1} dsDNA control (–) 0 h and (···) after 5 h; and 4 μM GL15 incubated with 100 μg mL^{-1} dsDNA during (—) 0, 1, 2, 3 and 5 h.

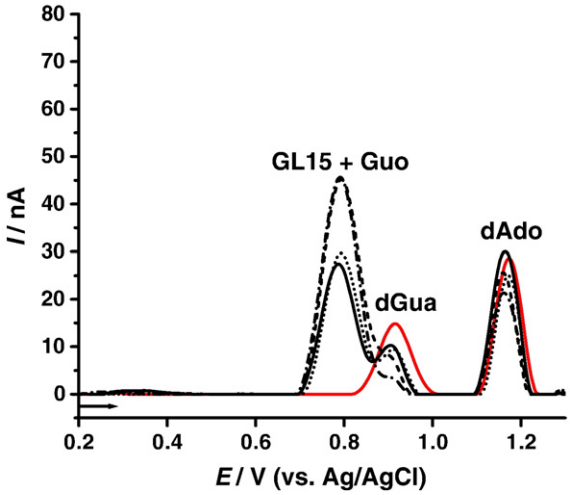

Fig. 6. DP voltammograms base-line corrected in pH = 7.0 0.1 M phosphate buffer of dsDNA-electrochemical biosensors (–) before and after incubation during: (—) 3, (•••) 5, (- - -) 7 and (-•-•-) 10 min in a solution of 50 μM GL15.

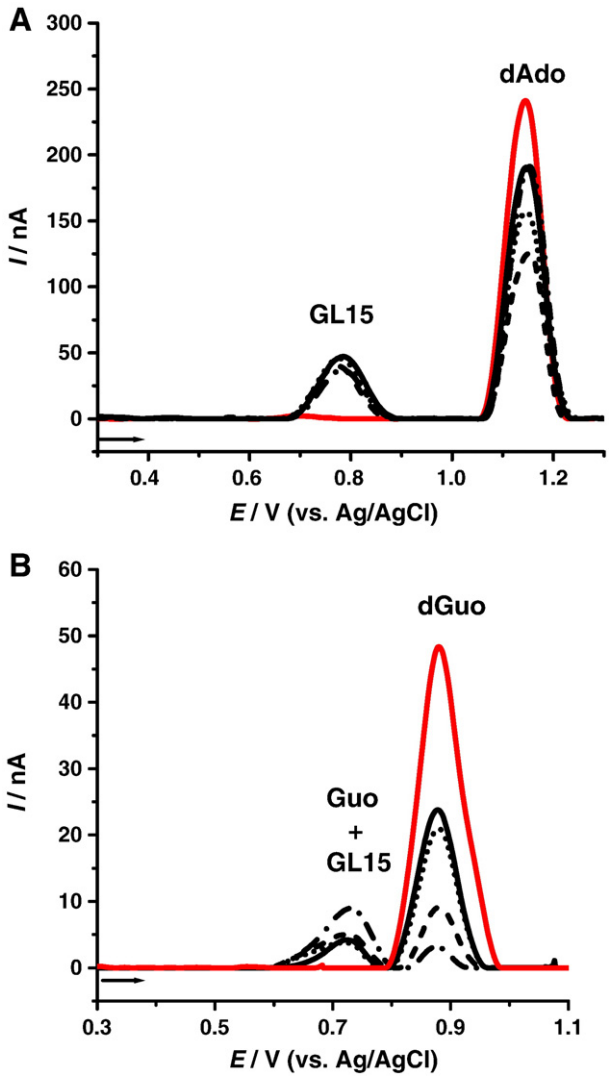

Fig. 7. DP voltammograms base-line corrected in pH = 7.0 0.1 M phosphate buffer: (A) poly[A] and (B) poly [G]-electrochemical biosensors (–) before and after incubation (—) 3, (•••) 5, (- - -)7 and (-•-•-) 10 min in a solution of 50 μM GL15.

Acknowledgments

Financial support from COST ACTION G4, Fundação para a Ciência e Tecnologia (FCT), PhD grant SFRH/BD/46026/2008 (A.D.R. Pontinha), project PTDC/QUI/098562/2008, POPH (co-financed by the European Community Funds FSE e FEDER/COMPETE), and CEMUC-R (Research Unit 285) is gratefully acknowledged. Work in the S.N. laboratory was supported by Programme Grant No. C129/A4489 from Cancer Research UK, and by the FP6 framework grant "Molecular Cancer Medicine" from the EU.

References

[1] T.M. Bryan, T.R. Cech, Telomerase and the maintenance of chromosome ends, Curr. Opin. Cell Biol. 11 (1999) 318–324.
[2] M. Mason, A. Schuller, E. Skordalakes, Telomerase structure function, Curr. Opin. Struct. Biol. 21 (2011) 92–100.
[3] A. De Cian, L. Lacroix, C. Douarre, N. Temime-Smaali, C. Trentesaux, J.-F. Riou, J.-L. Mergny, Targeting telomeres and telomerase, Biochimie 90 (2008) 131–155.
[4] L. Oganesian, T.M. Bryan, Physiological relevance of telomeric G-quadruplex formation: a potential drug target, BioEssays 29 (2007) 155–165.
[5] S.W.C. Hahn, S.A. Stewart, M.W. Brooks, S.G. York, E. Eaton, A. Kurachi, R.L. Beijersbergen, J.H.M. Knoll, M. Meyerson, R.A. Weinberg, Inhibition of telomerase limits the growth of human cancer cells, Nat. Med. 5 (1999) 1164–1170.
[6] J.W. Shay, W.E. Wright, Telomerase therapeutics for cancer: challenges and new direction, Nat. Rev. Drug Discov. 5 (2006) 577–584.
[7] M. Read, R.J. Harrison, B. Romagnoli, F.A. Tanious, S.H. Gowan, A.P. Reszka, W.D. Wilson, L.R. Kelland, S. Neidle, Structure-based design of selective and potent G quadruplex-mediated telomerase inhibitors, Proc. Natl. Acad. Sci. U. S. A. 98 (2001) 4844–4849.
[8] R.A. Hutchins, J.M. Crenshan, D.E. Graves, W.A. Denny, Influence of substituent modification on DNA binding energetic of acridine-based anticancer agents, Biochemistry 42 (2003) 13754–13761.
[9] F. Cuenca, O. Greciano, M. Gunaratnam, S. Haider, D. Munnur, R. Nanjunda, W.D. Wilson, S. Neidle, Tri- and tetra-substituted naphthalene diimides as potent G-quadruplex ligands, Bioorg. Med. Chem. Lett. 18 (2008) 1668–1673.
[10] C.M. Lombardo, I.S. Martínez, S. Haider, V. Gabelica, E. De Pauw, J.E. Moses, S. Neidle, Structure-based design of selective high-affinity telomeric quadruplex-binding ligands, Chem. Commun. 46 (2010) 9116–9118.
[11] S. Sparapani, S.M. Haider, F. Doria, M. Gunaratnam, S. Neidle, Rational design of acridine-based ligands with selectivity for human telomeric quadruplexes, J. Am. Chem. Soc. 132 (2010) 12263–12272.
[12] J.-H. Tan, L.-Q. Gu, J.-Y. Wu, Design of selective G-quadruplex ligands as potential anticancer agents, Mini-Rev. Med. Chem. 8 (2008) 1163–1178.
[13] P. Belmont, J. Bosson, T. Godet, M. Tiano, Acridine and acridone derivates, anticancer properties and synthetic methods: where are we now? Anticancer Agents Med. Chem. 7 (2007) 139–169.
[14] M.A. Read, S. Neidle, Structural characterization of a guanine—quadruplex ligand complex, Biochemistry 39 (2000) 13422–13432.
[15] M. Gunaratnam, O. Greciano, C. Martins, A.P. Reszka, C.M. Schultes, H. Morjani, J.-F. Riou, S. Neidle, Mechanism of acridine-based telomerase inhibition and telomere shortening, Biochem. Pharmacol. 7 (2007) 679–689.
[16] E. Salvati, C. Leonetti, A. Rizzo, M. Scarsella, M. Mottolese, R. Galati, I. Sperduti, M.F.G. Stevens, M. D'Incalci, M. Blasco, G. Chiorinoo, S. Bauwens, B. Horard, E. Gilson, A. Stoppacciarco, G. Zupi, A. Biroccio, Telomere damage induced by the G-quadruplex ligand RHPS4 has an antitumor effect, J. Clin. Invest. 117 (2007) 3236–3247.
[17] S.M. Haider, G.N. Parkinson, S. Neidle, Structure of a G-quadruplex–ligand complex, J. Mol. Biol. 326 (2003) 117–125.
[18] N.H. Campbell, G.N. Parkinson, A.P. Reszka, S. Neidle, Structural basis of DNA quadruplex recognition by an acridine drug, J. Am. Chem. Soc. 130 (2008) 6722–6724.
[19] J. Dai, M. Carver, L.H. Hurley, D. Yang, Solution structure of a 2:1 quindoline-c-MYC G-quadruplex: insights into G-quadruplex-interactive small molecule drug design, J. Am. Chem. Soc. 133 (2011) 17673–17680.
[20] A.D.R. Pontinha, S.C.B. Oliveira, A.M. Oliveira-Brett, Electrochemical oxidation of metolazone at a glassy carbon electrode, Electroanalysis 20 (2008) 2531–2536.
[21] S.M.A. Jorge, A.D.R. Pontinha, A.M. Oliveira-Brett, Electrochemical redox behaviour of omeprazole using a glassy carbon electrode, Electroanalysis 22 (2010) 625–631.
[22] S.C.B. Oliveira, M. Vivan, A.M. Oliveira-Brett, Electrochemical behavior of thalidomide at a glassy carbon electrode, Electroanalysis 20 (2008) 2429–2434.
[23] V.C. Diculescu, T.A. Enache, A.M. Oliveira-Brett, Electrochemical oxidation at a glassy carbon electrode of the anti-arrhythmia drug disopyramide, Anal. Lett. 40 (2007) 2860–2871.
[24] S.C.B. Oliveira, A.M. Oliveira-Brett, DNA-electrochemical biosensors: AFM surface characterisation an application to detection of in situ oxidative damage to DNA, Comb. Chem. High Throughput Screen. 13 (2010) 628–640.
[25] A.M. Oliveira-Brett, Electrochemistry for probing DNA damage, in: C.A. Grimes, E.C. Dickey, M.V. Pishko (Eds.), Encyclopedia of Sensors, American Scientific Publishers, USA, 2006, pp. 301–314.
[26] V.C. Diculescu, R.M. Barbosa, A.M. Oliveira-Brett, In situ sensing of DNA damage by a nitric oxide-releasing compound, Anal. Lett. 38 (2005) 2525–2540.
[27] A.M. Oliveira-Brett, V.C. Diculescu, Electrochemical study of quercetin–DNA interaction: part II. In situ sensing with DNA biosensor, Biochemistry 64 (2004) 143–150.
[28] C.M.A. Brett, A.M. Oliveira Brett, Electrochemistry: Principles, Methods and Applications, Oxford Science University Publications ed., Oxford, U.K., 1993.
[29] S.C.B. Oliveira, V.C. Diculescu, G. Palleschi, D. Compagnone, A.M. Oliveira-Brett, Electrochemical oxidation of ochratoxin A at a glassy carbon electrode and in situ evaluation of the interaction with deoxyribonucleic acid using an electrochemical deoxyribonucleic acid-biosensor, Anal. Chim. Acta 588 (2007) 283–291.
[30] M. Wainwright, Acridine—a neglected antibacterial chromophore, J. Antimicrob. Chemother. 47 (2001) 1–13.
[31] B.C. Baguley, L.P.G. Wakelin, J.D. Jacintho, P. Kovacic, Mechanisms of action of DNA intercalating acridine-based drugs: how important are contributions from electron transfer and oxidative stress? Curr. Med. Chem. 10 (2003) 2643–2649.
[32] A.-M. Chiorcea-Paquim, O. Corduneanu, S.C.B. Oliveira, V.C. Diculescu, A.M. Oliveira-Brett, Electrochemical and AFM evaluation of hazard compounds–DNA interaction, Electrochim. Acta 54 (2009) 1978–1985.
[33] S.C.B. Oliveira, A.M. Chiorcea-Paquim, S.M. Ribeiro, A.T.P. Melo, M. Vivan, A.M. Oliveira-Brett, In situ electrochemical and AFM study of thalidomide–DNA interaction, Bioelectrochemistry 76 (2009) 201–207.